Title	Shear Resistance of Sands under Undrained Condition and Potential for Rapid Flow Phenomena by Means of Ring Shear Tests
Author(s)	OKADA, Yasuhiko; SASSA, Kyoji; FUKUOKA, Hiroshi
Citation	京都大学防災研究所年報. B = Disaster Prevention Research Institute Annuals. B (2002), 45(B): 77-89
Issue Date	2002-04-01
URL	http://hdl.handle.net/2433/129088
Right	
Type	Departmental Bulletin Paper
Textversion	publisher

京都大学防災研究所年報 第45号 B 平成14年4月
Annuals of Disas. Prev. Res. Inst., Kyoto Univ., No. 45 B, 2002

Shear Resistance of Sands under Undrained Condition and Potential for Rapid Flow Phenomena by Means of Ring Shear Tests

Yasuhiko OKADA*, Kyoji SASSA, and Hiroshi FUKUOKA
* National Research Institute for Earth Science and Disaster Prevention

Synopsis

Shear resistance of two kinds of sands (fine silica and weathered granitic sands) mobilized within shear zone subjected to large shear displacement is examined. The undrained shear strengths at steady state of the specimens formed over the wide range of initial void ratios by ring shear tests are directly compared with those from the undrained triaxial compression tests. The steady state strengths in ring shear tests were smaller than those in triaxial compression tests due to grain crushing. While, small steady state strengths were observed by triaxial compression tests on dense fine silica sand in which there were clear shear surfaces and shear deformation must be concentrated on these surfaces to generate excess pore pressure. To express extent of apparent reduction of internal friction, the new parameter (P_f) was proposed as ratio of drained internal friction angle to apparent friction angle. Potential for rapid flow phenomena of employed two kinds of sands are clearly evaluated by P_f over the wide range of void ratio.

Keywords: Ring shear test; Grain crushing; Excess pore pressure; Shear resistance; Potential for rapid flow phenomena

1. Introduction

The rapid flow phenomena generally have the characteristics of high velocity and long travel distance along the moderately inclined slopes which are considered safe against landslides, and the subsequent severe damages and huge economic losses. The rapid flow phenomena are usually considered the expression of high excess pore pressure generation, in which the liquefaction of the soil mass or the specified thin shear zone would occur. Liquefaction was defined by Castro (1969) as:

"Liquefaction is a phenomenon wherein a mass of soil loses a large percentage of its shear resistance due to the excess pore pressure generation, when subjected to undrained monotonic, cyclic, or shock loading, and flows in a manner resembling a viscous liquid until the shear stresses acting on the mass are as low as or lower than the reduced shear resistance."

Liquefaction phenomenon has been focused by many researchers since the 1964 Niigata earthquake hit the south coast of Awa-Island Niigata, Japan, and the drastic effect on the slope stability was found in and reported (Seed and Lee 1966, Yoshimi 1977, Seed 1979, Finn 1981, and Ishihara et al. 1990, etc.). Accordingly, there are unnumbered experimental studies on liquefaction behaviour of sands and the undrained shear behaviour of sands has been rather elucidated. Castro (1969), Castro and Poulos (1977) and Poulos (1981) defined the steady state concept as the steady state for any mass of particles being that state in which the mass is continuously deforming at

a constant volume, constant normal effective stress, constant shear stress, and constant velocity. Based on their results, the steady state is independent of the initial soil structure, consolidation stress ratio, and the loading mode (cyclic or static) and is a function of initial void ratio only. This is one of the most appealing concepts such that the soil engineer confronting the soil liquefaction failure could judge the plots of the soil sample above the steady state line (on initial void ratio, e_0 – effective mean stress, p' diagram) at initial stress state would be susceptible to liquefaction and the plots below would be safe against it. Been and Jefferies (1985) proposed "state parameter" to express the properties of soil in relation to steady state. And as shown in Martin et al. (1975) and Groot et al. (1997), the trial of estimation in excess pore pressure generation under undrained condition from the drained test results were also conducted by using simple shear and triaxial compression tests. However, these studies were within the quite limited range of shear displacement and the effect of the formation of shear surface and the resulting grain crushing on the liquefaction characteristics was barely taken into consideration. Furthermore, Sassa (1996) and Sassa et al. (1996) showed the conspicuous effect of grain crushing along the shear surface of ring shear test on excess pore pressure generation, and proposed the new concept of "sliding-surface liquefaction." This concept has the point of breakthrough that sliding-surface liquefaction could take place in medium dense or even dense states as well as loose one to cause rapid flow phenomena.

In this study, the shear resistances of the two kinds of sand under undrained condition by the conventional triaxial compression tests and ring shear tests which can give the limitless shear displacement are examined over the wide range of initial void ratio and the potential against rapid flow phenomena is discussed with the parameter of potential for rapid flow phenomena (P_f) which is the ratio of internal friction angle under drained condition to apparent friction angle mobilized under undrained condition.

2. Characteristics of Samples

In this research, fine silica (silica sand no.8) and weathered granitic sands (Osaka-group coarse sandy soils) were employed.

Silica sand no.8 is a uniform sandy silt, consisting of 92 through 98 percent quartz and a little amount of feldspar, the grains being sub-angular to angular with the mean diameter D_{50} = 0.048 mm, a uniformity coefficient Uc = 2.8, and specific gravity Gs = 2.63.

Osaka-group coarse sandy soils, Pliocene to Mid-Pleistocene limnic and marine deposits of weathered granitic sands (Ichihara 1996), are widely distributed in the Kansai area, Japan. The sampling site was at the headscarp of the Takarazuka Golf Course landslide, which was triggered by the 1995 Hyogo-ken Nanbu earthquake. The sampling point depth was about 4 m. Totally, more than 1 ton of soil were removed by an excavating machine. The composition of this sandy soil was weathered granite, consisting of 77 percent of quartz and 23 percent of feldspar, the grains being angular with the mean diameter D_{50} = 1.2 mm, a uniformity coefficient Uc = 3.4, and specific gravity Gs = 2.61. The Takarazuka Golf Course landslide is a typical of long run-out rapid flow phenomenon (Fukuoka et al. 1997) and it may have occurred under the saturated undrained condition (Sassa et al. 1996, and Okada et al. 2000).

Figure 1 presents the grain size distribution curves of two kinds of sand employed in this study.

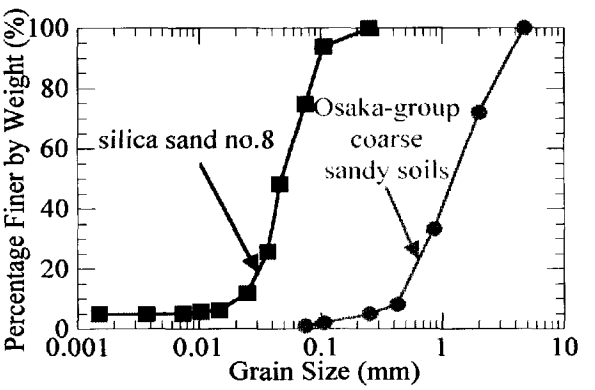

Fig. 1 Grain size distribution curves of employed samples

3. Apparatus and Test Procedure

3.1 Apparatus

The triaxial compression test apparatus used accepts specimens with a nominal height of 200 mm and diameter of 100 mm. Air pluviation (rained sand through air) was used to prepare the sample because it provides a more uniform specimen (Gilbert and Marcuson 1988, and Mooney et al. 1998) and forms

specimens with the lowest resistance to liquefaction (Mulilis et al. 1977, Ishihara 1993, and Sukumaran et al. 1996). Tamping was used to form medium dense through dense specimens.

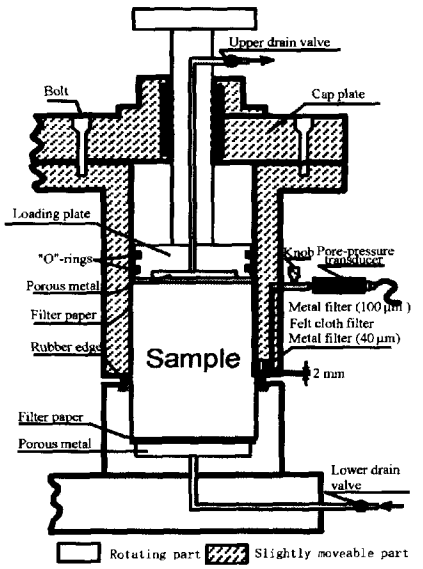

Fig. 2 A half section of undrained shear box and pore pressure measurement

The ring shear test apparatus used is the fifth version (DPRI-5; first used in 1996) of a family of ring shear test apparatuses developed at the Disaster Prevention Research Institute, Kyoto University. It is an improvement on DPRI-3 (Sassa 1995) in that it provides better pore pressure measurement. This test apparatus enables us to simulate all different kinds of static or cyclic loading under speed- or stress-controlled condition on the donut-shaped specimens with 180 mm in outer diameter and 120 mm in inner diameter. The nominal specimen height during shearing is about 60 mm and the shear surface locates at about the centre of the specimen. Figure 2 illustrates a half section of undrained shear box and pore pressure measurement system (DPRI-5). It should be mentioned that, in order to prevent the leakage of water and soil from the gap between the upper and lower halves of the shear box, a rubber edge was glued to the upper surface of the lower half of the shear box. In addition, the contact surface was turned on a lathe to remove any unevenness. After assembling the ring shear test apparatus, the contact force was kept constant at 1.4 kN. Teflon was sprayed on the rubber edge to decrease friction between the contact surface, and silicon grease was spread on it to obtain the complete undrained condition. The free-fall deposition method was used to prepare the loose specimen. The oven-dried sample was poured by the cup into the shear box. Tamping and overconsolidation were conducted to form the medium dense and dense specimens.

3.2 Test Procedure

After setting up the specimens for both of triaxial compression and ring shear tests, the specimens were saturated by means of carbon dioxide and de-aired water as following;

(1) Carbon dioxide was flushed (for 1 hour) from the bottom into the specimens to replace the air.

(2) De-aired water was percolated through the specimen for about 12 hours.

The pore pressure parameter, B (Skempton 1954), was measured by the undrained triaxial compression test in order to check the degree of saturation of the specimen. Pore pressure parameter, B_D, proposed by Sassa (1988 and 1995) for the undrained direct shear condition, was measured in undrained ring shear tests. B_D is approximately equal to B for uniform soils. The B and B_D values are derived in equations (1) and (2).

$$B = \Delta u / \Delta\sigma_3 \qquad (1)$$

$$B_D = \Delta u / \Delta\sigma \qquad (2)$$

where Δu is the excess pore pressure under undrained condition, $\Delta\sigma_3$ the increment of minor principal stress, and $\Delta\sigma$ the increment of normal stress. In this study, all of the specimens used in the analyses were with B or B_D values larger than 0.95 and were regarded as fully saturated specimens.

In order to investigate the influence of initial void ratio on the undrained shear strength, the specimens at the wide range of initial void ratio for speed-controlled triaxial compression tests (O_{t1} through O_{t9} on Osaka-group coarse sandy soils and S_{t1} through S_{t10} on silica sand no.8) and speed-controlled ring shear tests (O_{r1} through O_{r3} on Osaka-group coarse sandy soils and S_{r1} through S_{r8} on silica sand no.8) were formed at total normal stress of approximately 197 kPa. Axial speed in the triaxial compression tests was 0.05 mm/sec for up to 50 mm axial displacement. Shear speed in the ring shear tests was 0.3 mm/sec up to 1 m shear displacement, after which it was held at 3.0 mm/sec up to as much as 10

Table 1 Test identification number and condition

Test No.	Sample	Apparatus	σ_3 or σ_0 (kPa)	e_0	B or B_D	Drainage condition
S_{t1}	Silica sand no.8	Triaxial compression	198	1.11	0.96	Undrained
S_{t2}			198	1.07	0.96	
S_{t3}			198	1.05	0.96	
S_{t4}			198	1.01	0.95	
S_{t5}			197	1.00	0.96	
S_{t6}			198	0.96	0.95	
S_{t7}			197	0.92	0.95	
S_{t8}			197	0.90	0.95	
S_{t9}			199	0.88	0.95	
S_{t10}			197	0.86	0.96	
S_{r1}		Ring shear	197	1.10	0.96	
S_{r2}			198	1.08	0.96	
S_{r3}			197	1.07	0.96	
S_{r4}			197	1.02	0.95	
S_{r5}			197	0.98	0.95	
S_{r6}			198	0.93	0.96	
S_{r7}			197	0.89	0.95	
S_{r8}			197	0.86	0.96	
O_{t1}	Osaka-group coarse sandy soils	Triaxial compression	196	0.76	0.96	Undrained
O_{t2}			196	0.73	0.96	
O_{t3}			195	0.67	0.96	
O_{t4}			196	0.61	0.96	
O_{t5}			196	0.60	0.96	
O_{t6}			196	0.58	0.95	
O_{t7}			197	0.57	0.95	
O_{t8}			196	0.55	0.95	
O_{t9}			196	0.52	0.95	
O_{r1}		Ring shear	196	0.75	0.96	
O_{r2}			195	0.61	0.95	
O_{r3}			196	0.55	0.95	

m shear displacement. Table 1 summarizes the test numbers and conditions.

4. Comparative analysis of the undrained shear strengths from ring shear and triaxial compression tests

4.1 Conventional liquefaction and sliding-surface liquefaction

Sassa (1996) and Sassa et al. (1996) proposed the concept of sliding-surface liquefaction based on their studies on landslides triggered by the 1995 Hyogo-ken Nanbu earthquake, using the undrained ring shear tests. Liquefaction is normally generated by destruction of the meata-stable soil skeletal structure of a loose saturated soil mass. Grain crushing is not required. The stress path usually indicates collapse failure before the failure line is reached. On the contrary, sliding-surface liquefaction occurs as shear displacement progresses. Destruction of the loose structure is not always necessary. Excess pore pressure is generated by grain crushing and comminution within the shear zone. If grains are crushed and comminuted along the sliding surface, causing the volume shrinkage, sliding-surface liquefaction is reckoned to occur at any void ratio, even in the very dense state. The stress path in sliding-surface liquefaction necessarily reaches a failure line, thereafter moving left-downward along a failure line.

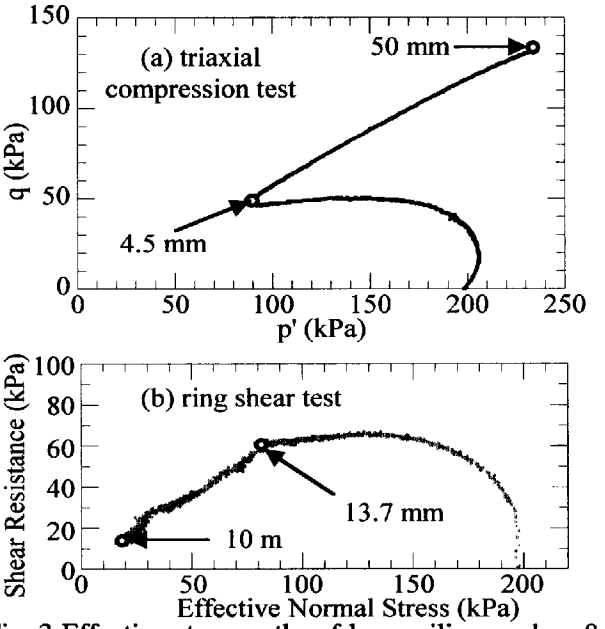

Fig. 3 Effective stress paths of loose silica sand no.8. (a)triaxial compression test (S_{t1}:e_0=1.11), (b)ring shear test (S_{r1}:e_0=1.10)

As it is actually impossible to show all of the results, in this paper only typical test results on the specimen at loose, medium dense, and dense state is illustrated in the form of effective stress paths. Figure 3(a) and (b) shows the effective stress paths of loose silica sand no.8 specimens in triaxial compression test (S_{t1}: e_0 = 1.11) and ring shear test (S_{r1}: e_0 = 1.10). Numeral in the figure expresses axial and shear displacements, respectively. In ring shear test, excess pore pressure was generated monotonically, and quite small shear resistance at 10 m shear displacement was observed after the effective stress path reached a failure line at 13.7 mm shear displacement. Sliding-surface liquefaction took place, with the progress of shear displacement to cause grain crushing and resulting excess pore pressure generation (Sassa 1996 and Sassa et al. 1996). The effective stress path came to a standstill when the effective normal stress became so small that it caused no further grain crushing. Whereas, pore pressure in triaxial compression test was increased first with deviator stress showing a very small temporary peak, however, at 4.5 mm axial displacement of phase transformation point defined by Ishihara et al. (1975) to exhibit quasi steady state (Alarcon-Guzman et al. 1988), it was decreased to regain the high deviator stress, q' $(=(\sigma_1' - \sigma_3')/2)$ at 50 mm axial displacement at which test was ceased. Accordingly, the loose silica sand no.8 at almost the same void ratio, sliding-surface liquefaction was observed in the ring shear test on the one hand, while, only limited liquefaction (Casagrande 1976) behaviour was obtained in triaxial compression test. The effective stress paths of loose Osaka-group coarse sandy soils (Test O_{t1}: e_0 = 0.76 and O_{r1}: e_0 = 0.75) are shown in Fig. 4(a) and (b). In both tests, excess pore pressure continued to monotonically increase, resulting in very low deviator stress in triaxial compression test or shear resistance in ring shear test being observed at the end of the tests. The notable difference is that a failure line appeared in the effective stress path in Test O_{r1}, however, is not observed in Test O_{t1}. The effective stress path for Test O_{t1} was typical of conventional liquefaction. It reached peak, q' at 1.8 mm axial displacement after which flow deformation was generated and the effective stress path moved without reaching any failure line. As for loose Osaka-group coarse sandy soils at almost the same void ratio, sliding-surface liquefaction was observed in ring shear test and conventional liquefaction phenomenon was produced by triaxial compression test, indicative that different types of liquefaction were taking place.

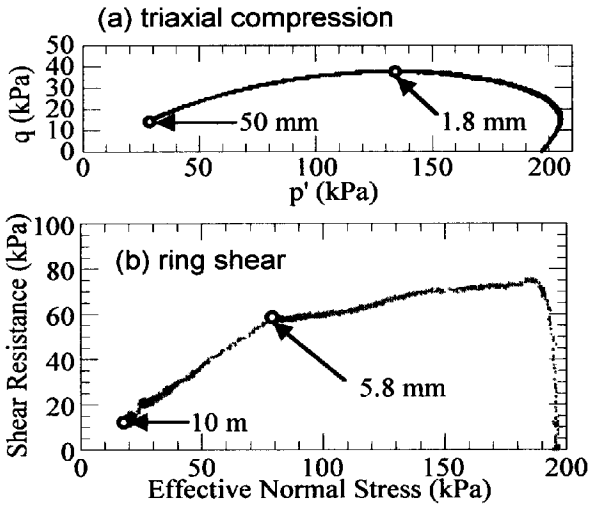

Fig. 4 Effective stress paths of loose Osaka-group coarse sandy soils. (a)triaxial compression test (O_{t1}:e_0=0.76), (b)ring shear test (O_{r1}:e_0=0.75)

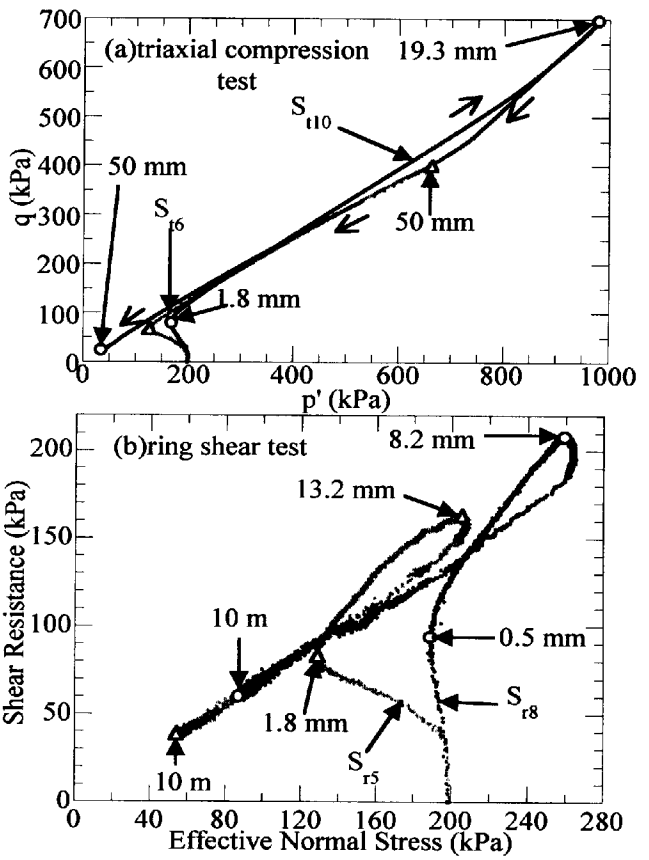

Fig. 5 Effective stress paths of medium dense and dense silica sand no.8. (a)triaxial compression test (S_{t6}:e_0=0.96, S_{t10}:e_0=0.86), (b)ring shear test (S_{r5}:e_0=0.98, S_{r8}:e_0=0.86)

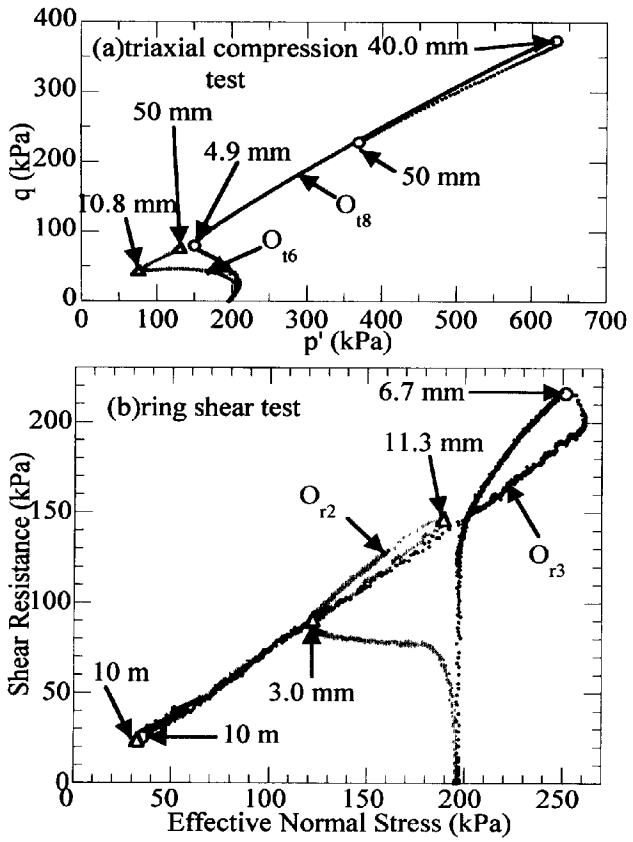

Fig. 6 Effective stress paths of medium dense and dense Osaka-group coarse sandy soils. (a)triaxial compression test (O_{t6}:e_0=0.60, O_{t8}:e_0=0.55) (b) ring shear test (O_{r2}:e_0=0.61, O_{r3}:e_0=0.55)

The different undrained shear behaviour of the both specimens in triaxial compression tests and ring shear tests undoubtedly due to the difference in the shearing actions of the two types of shear apparatuses. The triaxial compression test produced homogeneous deformation within the whole specimens, whereas, the direct shear condition along a specified shearing surface was given in the ring shear tests causing much more grain crushing within shear zone.

4.2 Excess pore pressure generation associated with shear deformation along shear surface

The effective stress paths of medium dense silica sand no.8 (Test S_{t6}: e_0 = 0.96) and dense (Test S_{t10}: e_0 = 0.86) in triaxial compression tests and medium dense (Test S_{r5}: e_0 = 0.98) and dense (Test S_{r8}: e_0 = 0.86) found in ring shear tests are presented in Fig. 5(a) and (b). The shape of the effective stress paths of Test S_{r5} and S_{r8} found in ring shear tests were similar. The effective stress paths moved left-ward to reach phase transformation (PT) and going right-upward to show peak shear resistance, after which they proceeded left-downward to low shear resistance along a failure line due to excess pore pressure generation by grain crushing. Shear resistances at peak and 10 m shear displacement were in inverse relation to the void ratio and they showed sliding-surface liquefaction behaviour. Whereas, Tests S_{t6} and S_{t10} showed quite different behaviour such that S_{t6} regained quite high deviator stress at 50 mm axial displacement and S_{t10} exhibited quite low deviator stress after effective stress path showed very high peak deviator stress and climbed down along a failure line. The effective stress path of S_{t10} was similar to that of sliding-surface liquefaction found in ring shear tests. Generally, it is recognized that, the smaller the void ratio, the higher the deviator stress in the sandy soils at steady state, and the test results of loose and medium dense silica sand no.8 specimens (S_{t1} and S_{t6}) were in accordance with it. However, dense specimen (Test S_{t10}) produced the lower deviator stress than even that of loose specimen. Figure 6(a) and (b) illustrates the effective stress paths of medium dense and dense Osaka-group coarse sandy soils in triaxial compression tests (Tests O_{t6} and O_{t8}) and in ring shear tests (Tests O_{r2} and O_{r3}). As found in medium dense and dense silica sand no.8 specimens of ring shear tests, shear resistances at peak and 10 m shear displacement of medium dense and dense specimens (Test O_{r2} and O_{r3}) were inversely proportional, and the effective stress paths moved left-downward along a failure line to very low shear resistance. Sliding-surface liquefaction took place with the progress of shear displacement due to grain crushing within shear zone. While, in the medium dense specimen of triaxial compression test (Test O_{t6}), the effective stress path moved left-downward considerably at the beginning of the test, however, strain hardening behaviour was observed to regain the strength at 50 mm axial displacement. Dense specimen (Test O_{t8}) showed the same tendency found in Test O_{r2}, like the effective stress path showed phase transformation at 4.7 mm axial displacement and moved right-upward, however, it reversed its direction at 46.3 mm axial displacement proceeding left-downward along a failure line associated with excess pore pressure generation. Due to the limitation of the linear transducer for axial displacement measurement, test was finished at 50 mm axial displacement and

deviator stress exhibited about 230 kPa. However, if it was possible to continue the test further, the effective stress path would go left-downward more to show much low deviator stress.

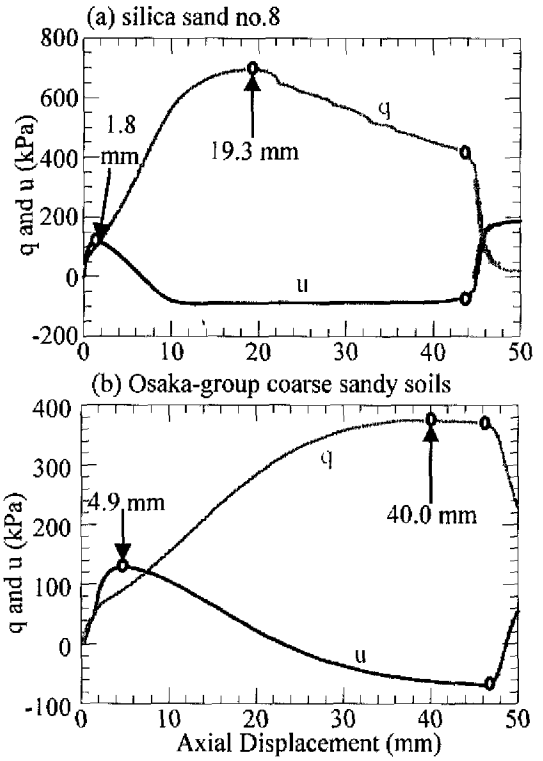

Fig. 7 Relationship of deviator stress (q) and pore pressure (u) versus axial displacement of dense specimens. (a) silica sand no.8 (S_{t10} : e_0=0.86), (b) Osaka-group coarse sandy soils (O_{t8} : e_0=0.55)

In general, much lower shear resistances were obtained in ring shear tests than those in triaxial compression tests, except for dense silica sand no.8 and loose Osaka-group coarse sandy soils. As stated, this undoubtedly is due to the difference in the shearing actions of two types of apparatuses. Smaller displacements between soil particles generally occur in the homogeneous deformation with limitation of axial displacement that takes place in triaxial compression tests, whereas, much larger displacements are produced between soil particles along the shear surface during shearing in ring shear tests. With formation of a shear surface, excess pore pressure are generated due to grain crushing and give rise to lower shear resistances in ring shear tests than those in triaxial compression tests. The dense specimens (Test S_{t10} and O_{t8}) showed marked regeneration of excess pore pressure and the decrease of deviator stress in relation to axial displacement as presented in Fig. 7(a) and (b). The deviator stress of Test S_{t10} had peak at 19.3 mm axial displacement and then it decreased gradually up to 43.8 mm axial displacement, followed by sudden reduction of deviator stress with the rapid excess pore pressure generation. And the deviator stress of Test O_{t8} showed peak at 40.0 mm axial displacement and had the sudden reduction at 46.3 mm axial displacement. Photo 1(a) and (b) presents the those dense cylindrical specimens in the triaxial compression tests (Tests S_{t10} and O_{t8}) with definite shear surfaces formed at about 50 mm axial displacement. In this stage, shear deformation of the specimens may have been concentrated along formed shear surfaces.

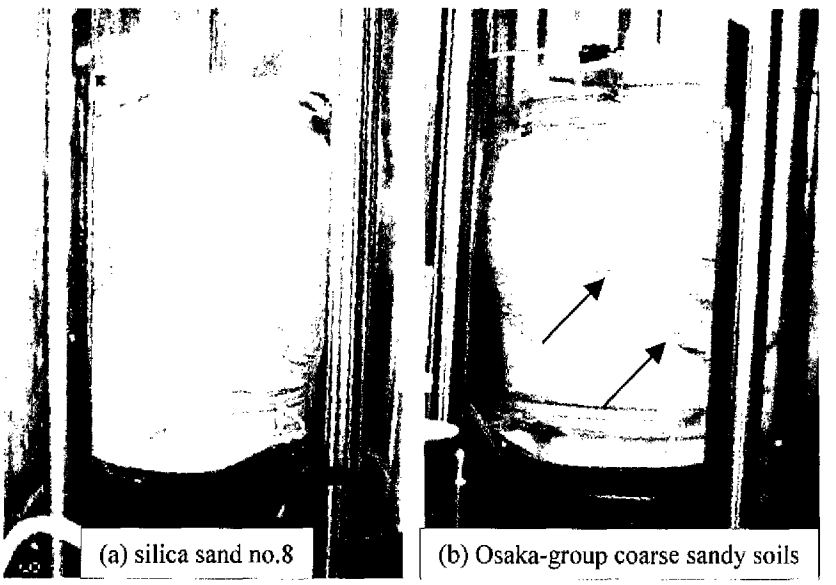

Photo. 1 Shear surfaces formed in the cylindrical dense specimens.
(a) silica sand no.8 (S_{t10} : e_0 = 0.86), and (b) Osaka-group coarse sandy soils (O_{t8} : e_0 = 0.55)

Therefore, considerable sliding undoubtedly occurred along these shear surfaces, and the grains may have been very much crushed as in ring shear tests. Excess pore pressure regeneration in this case probably was due to grain crushing on the shear surfaces, and the mechanism was the same as that of the sliding-surface liquefaction found in the undrained ring shear tests.

4.3 Mobilized peak and steady state strengths and potential for rapid flow phenomena

The peak shear strengths and steady state strengths ought to be some of the most basilical shear parameters to determine the undrained shear behaviour such that they introduce the concepts of the initiation and consequence or motion of liquefaction failure to generate rapid flow phenomena. Figure 8(a) and (b) shows the relationship between initial void ratio and peak strengths of silica sand no.8 (Tests S_{t1} through S_{t10} and S_{r1} through S_{r8}) and Osaka-group coarse sandy soils (Tests O_{t1} through O_{t9} and O_{r1} through O_{r3}). It should be mentioned that, in order to compare the results of triaxial compression tests directly with ring shear tests, shear resistances in the triaxial compression tests are the values on the theoretical shear surfaces being formed in the cylindrical specimen calculated through equation (3) as following.

$$\tau^{t}_{peak} = q_{peak} \times \cos(\sin^{-1}(q_{peak} / p'_{peak})) \qquad (3)$$

in which τ^{t}_{peak} is peak shear resistance on the theoretical shear surface in triaxial compression test; q_{peak} peak deviator stress; and p'_{peak} effective mean stress at peak, respectively. The smaller void ratio generated larger peak strengths in both of the ring shear tests and triaxial compression tests for each specimen. Given the void ratio being the same, the smaller peak strengths were obtained in ring shear tests than in triaxial compression tests in silica sand no.8, in contrast, triaxial compression tests produced smaller peak strengths than those in ring shear tests in Osaka-group coarse sandy soils except for dense state. It means that silica sand no.8 sample are easier to suffer from liquefaction failure in the direct shear condition of ring shear tests than in the homogeneous deformation of triaxial compression tests, on the contrary, Osaka-group coarse sandy soils generally showed the opposite tendency. The difference might be dependent on the grain size distribution, crushability, and mineral component, etc.

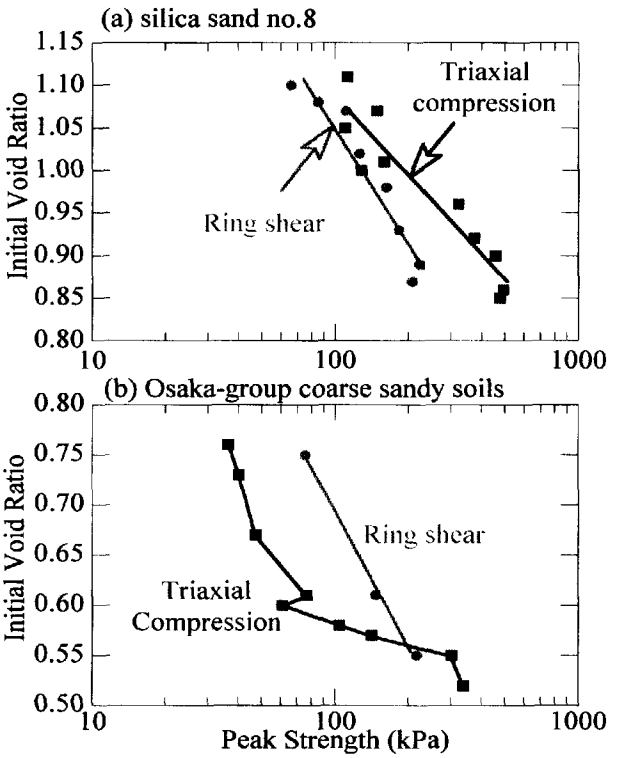

Fig. 8 Relationship between initial void ratio and peak shear strengths by triaxial compression and ring shear tests. (a) silica sand no.8, and (b) Osaka-group coarse sandy soils

Figure 9(a) and (b) presents the relationship of steady state strengths versus initial void ratio of in silica sand no.8 (Tests S_{t1} through S_{t10} and S_{r1} through S_{r8}) and Osaka-group coarse sandy soils (Tests O_{t1} through O_{t9} and O_{r1} through O_{r3}). Shear resistance at steady state in triaxial compression tests was calculated at 50 mm axial displacement at which tests were ceased by equation (4) as follows.

$$\tau^{t}_{ss} = q_{(la=50mm)} \times \cos(\sin^{-1}(q_{(la=50mm)} / p'_{(la=50mm)})) \qquad (4)$$

where τ^{t}_{ss} is shear resistance at steady state in triaxial compression test; $q_{(la=50mm)}$ deviator stress at 50 mm axial displacement; $p'_{(la=50mm)}$ effective mean stress at 50 mm axial displacement, respectively. Shear resistance at steady state for ring shear tests were plotted at 10 m shear displacement at

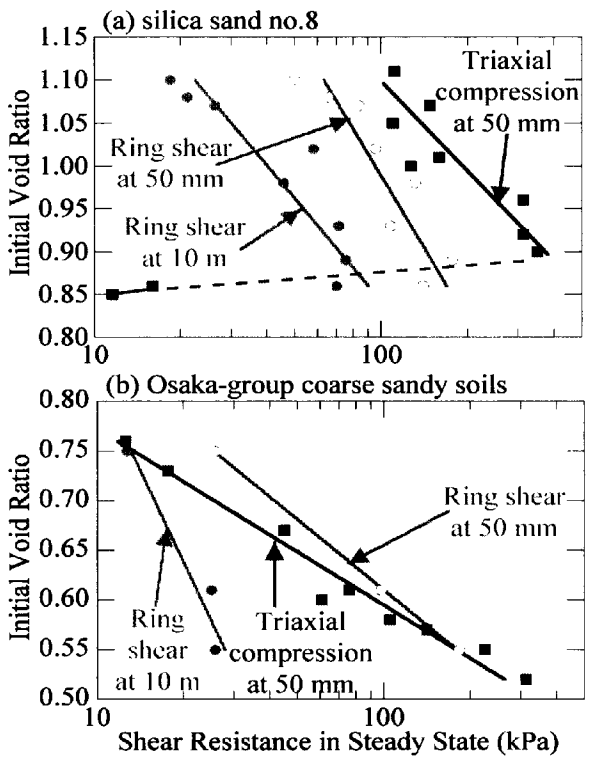

Fig. 9 Relationship between initial void ratio and shear resistance in steady state by triaxial compression and ring shear tests. (a) silica sand no.8, and (b) Osaka-group coarse sandy soils

which tests were ceased, and as a reference, the shear resistance at 50 mm shear displacement were also plotted in the figure to compare shear resistance at steady state from triaxial compression tests at similar shear displacement. Except for dense silica sand no.8 specimen, steady state strengths were also inverse relation to initial void ratio, as was seen in peak strengths. It was found that, shear resistance at 50 mm shear displacement as well as steady state strengths at 10 m shear displacement were smaller than steady state strengths in triaxial compression tests as for silica sand no.8 sample, except for except for dense specimens. Whereas, steady state strengths of Osaka-group coarse sandy soils in triaxial compression tests were slightly smaller than shear resistance at 50 mm shear displacement in ring shear tests and larger than steady state strengths in ring shear tests, except for loose specimen. As mentioned before, these may be due to the difference of grain size distribution, crushability, and mineral component, etc. However, it can be said that the steady state strengths at 10 m shear displacement in ring shear tests after sliding-surface liquefaction took place were, in general, smaller than those from triaxial compression tests. And the point to mention is that quite good correlation between three series of shear resistance and initial void ratio were observed, and shear resistance could be approximated by respective straight lines. It is worth while noticing that there is a controversy on the existence of the unique steady state line (Hanzawa 1980, Miura and Toki 1982, Kuerbis and Vaid 1988, Vaid et al. 1990, Riemer and Seed 1997, and Mooney et al. 1998, etc.) and on the difference between steady state line and critical state line (Poulos 1981, Sladen et al. 1985, Alarcon-Guzman 1988, and Been et al. 1991, Yoshimine and Ishihara 1998, etc.). The consensus that the steady state depends on the stress path (compression or extension in triaxial tests) and that the steady state line and critical state line are the same, seem to be prevailing. Hence, the straight lines found in Fig 9(a) and (b) are regarded as in steady state. Matos (1988) investigated the influence of uniformity coefficient of the specimens on the steady state line using the same crushed quartz sands by means of triaxial compression tests. A specimen having a different grain size distribution has a different steady state line in $e_0 - p'$ diagram such that the steady state line shifts downward in a greater uniformity coefficient. However, it should be remembered that Poulos (1981) insisted that the steady state could be obtained only after all particle crushing was complete and this condition could be attained only at larger strains – well beyond those that can be reached in triaxial tests. As well-known, the grain crushing in the triaxial compression tests are limited, whereas in ring shear tests the grains along the shear surface were crushed as much as possible when sliding-surface liquefaction took place to reach steady state. Along this line of thought, steady state line should shift leftward, as grain crushing proceeds, to reach ultimate position when grain crushing along the shear surface is terminated. Accordingly, the steady state line determined by the ring shear tests subjected to large shear displacement after the sliding-surface liquefaction took place can be proposed as "ultimate steady state line" which gives the undrained shear strengths in the long run-out landslides. It should be mentioned about the fact that steady state strengths at 50 mm axial displacement in the triaxial compression tests on dense silica sand no8 specimens presented smaller values than those on ultimate steady state line

from ring shear tests. This should be due to the fact that, in those cases, several shear surfaces (see Photo 1(a)) were formed in the cylindrical specimens and shear deformation took place along those surfaces not only one surface to generated excess pore pressure simultaneously by grain crushing.

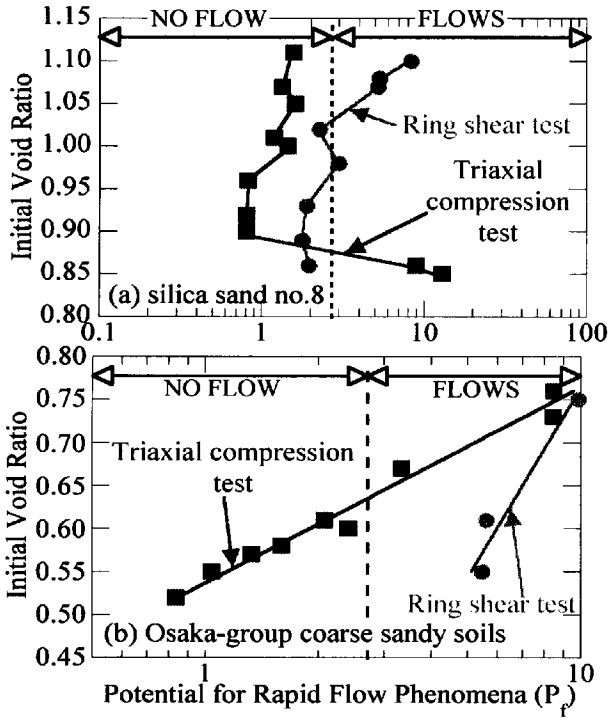

Fig. 10 Relationship between initial void ratio and potential for rapid flow phenomena (P_f) from triaxial compression and ring shear tests. (a) silica sand no.8, and (b) Osaka-group coarse sandy soils

4.4 Potential for rapid flow phenomena

Sassa (2000), and Sassa et al. (2001) proposed the criterion about the rapid flow phenomena such that the rapid flow phenomena take place when mobilized apparent friction angles become smaller than 15 degrees. The potential for rapid flow phenomena could be evaluated by the apparent reduction of internal friction angle of soils during sliding motion. Usually the sandy soils have the similar internal friction angles under drained condition of about 30 through 40 degrees, however, the apparently mobilized friction angle (apparent friction angle) during sliding motion are quite different for different samples. Therefore, the new parameter "potential for rapid flow phenomena" is proposed as following to express the reduction potential of apparent internal friction angle during sliding motion for flow potential evaluation.

$$P_f = \frac{\tan\phi_d}{\tan\phi_a} \qquad (5)$$

in which P_f is potential for rapid flow phenomena, ϕ_d internal friction angle under drained condition, ϕ_a apparent friction angle, respectively. When rapid flow phenomena occur, the apparent friction angles were small, leading to the bigger potential for raid flow phenomena. Higher potential for rapid flow phenomena would explain the transition from "slide" to "flow" of landslides. And it is considered that internal friction angle under drained condition (ϕ_d) and effective internal friction angle under undrained condition (ϕ_u) are nearly equal, potential for rapid flow phenomena (P_f) would be calculated using effective internal friction angle under undrained condition (ϕ_u).

The potential for rapid flow phenomena of ring shear and triaxial compression tests versus initial void ratio are shown in Fig. 10, in which (a) presents the results of silica sand no.8 and (b) Osaka-group coarse sandy soils, respectively. Based on the criterion to judge the flow behaviour (Sassa 2000, and Sassa et al. 2001), assuming the effective internal friction angle under undrained condition being 36 degrees, potential for rapid flow phenomena would occur with P_f smaller than 2.7 when apparent friction angle is set at 15 degrees. Hence, the dotted line at 2.7 of potential for rapid flow phenomena was drawn in the figure as a reference. In the area on the right side of this line, rapid flow phenomena would be resulted in, on the contrary in the area on the left side, no flow. As seen in general, the greater potential for rapid flow phenomena were observed when initial void ratio were larger and ring shear tests in each sample. As for Osaka-group coarse sandy soils, ring shear tests generated rapid flow phenomena irrespective of initial void ratio, whereas triaxial compression test produced rapid flow phenomena in rather loose state at void ratio greater than about 0.67 (see Fig. 9(a)). While, loose silica sand no.8 specimen in ring shear tests and dense specimens in triaxial compression tests generated rapid flow phenomena . And in medium dense through dense specimens in ring shear tests and loose through medium dense specimens in triaxial compression tests, no flow was obtained.

Based on the test results presented above, Osaka-group coarse sandy soils have high potential to

suffer from rapid flow phenomena, irrespective of initial void ratio under the direct shear condition of ring shear tests. Whereas, in medium dense through dense state, the low potential of rapid flow phenomena was obtained in homogeneous deformation of triaxial compression tests. Accordingly, the greater potential for rapid flow phenomena was obtained in direct shear condition which formed the shear surface in the specimens on which grain crushing should take place considerably to generate excess pore pressure, than in homogeneous deformation. While in silica sand no.8 sample presented rather small potential for rapid flow phenomena such that in only loose state by ring shear tests and in dense state by triaxial compression tests rapid flow phenomena were observed. But in this case also, it would be mentioned that the potential for rapid flow phenomena was influenced by grain crushing characteristics on the shear surface.

5. Concluding remarks

Based on the test results of the series of the undrained ring shear tests and another series of undrained triaxial compression tests on silica sand no.8 and Osaka-group coarse sandy soil samples formed over the wide range of initial void ratio, the followings could be drawn.

(1) The quite different undrained shear behaviour was obtained from ring shear tests and triaxial compression tests on the specimens at almost the same void ratio. The undrained ring shear tests generated sliding surface liquefaction behaviour much more than triaxial compression tests, irrespective of initial void ratio and samples. This undoubtedly is due to the difference in the sliding actions of the tow types of shear apparatuses.

(2) To evaluate the extent of apparent reduction of internal friction angle during shearing, the new parameter of potential for rapid flow phenomena (P_f) was proposed as the ratio of internal friction angle under drained condition to the apparent friction mobilized under undrained condition.

(3) Direct comparison of shear resistance in sogenannt steady state from undrained ring shear and triaxial compression tests, it was revealed the ring shear tests, in general, generated smaller steady state strengths and larger potential for rapid flow phenomena (P_f) than triaxial compression tests. Since the steady state in ring shear tests was reached after all particle crushing having been terminated ultimately and it is quite different from that of the triaxial compression tests, it was proposed as "ultimate steady state" in which the undrained shear strengths and the potential for rapid flow phenomena for study of long run-out landslides ought to be evaluated.

(4) As is usual in the studies on steady state, steady state strengths of silica sand no.8 in triaxial compression tests were generally proportional to initial void ratio. However, the dense specimens produced regeneration of excess pore pressure to make the effective stress paths move left-downward along a failure line to very small steady state point. It was assured that the shear deformation accompanied by grain crushing along several shear surfaces formed in the cylindrical specimens regenerated excess pore pressure as the same mechanism of sliding-surface liquefaction.

Acknowledgements

The authors wish to thank Mr. Kondo of the Disaster Prevention Research Institute, Kyoto University for his useful advice and a great help for troubleshooting of the ring shear and triaxial compression apparatuses. Heartfelt thanks also are extended to former and present postgraduate students in the Landslide Section, DPRI, Kyoto University, for their suggestion and discussion throughout our study.

References

Alarcon-Guzman, A., Leonards, G.A., and Chameau, J.L. (1988): Undrained monotonic and cyclic strength of sands. Journal of Geotechnical Engineering Division, ASCE, **114**(10): 1089-1109.

Been, K., and Jefferies, M.G. (1985): A state parameter for sands. Géotechnique, **35**(2): 99-112.

Been, K., Jefferies, M.G., and Hachey, J. (1991): The critical state of sand. Géotechnique, **41**(3): 365-381.

Casagrande, A. (1976): *Liquefaction and Cyclic Deformation of Sands – A Critical Review*. Harvard Soil Mechanics Series, No. 88. Harvard University, Cambridge, Massachusetts.

Castro (1969): *Liquefaction of Sands*. Ph. D. Thesis, Harvard Soil Mechanics Series, No.81. Harvard University, Cambridge, Massachusetts.

Castro, G., and Poulos, S.J. (1977): Factors affecting liquefaction and cyclic mobility. Journal of Geotechnical Engineering Division, ASCE, **103**(GT6): 501-516.

Finn, W.D.L. (1981): Liquefaction potential: developments since 1976. *In* Proceedings of the 1st International Conference on Recent Advances in Geotechnical Earthquake Engineering and Soil Dynamics, St. Louis, **2**: 655-681.

Fukuoka, H., Sassa, K., and Scarascia-Mugnozza, G. (1997): Distribution of landslides triggered by the 1995 Hyogo-ken Nanbu Earthquake and long runout mechanism of the Takarazuka golf course landslide. Journal of Physics of the Earth, **45**: 83-90.

Gilbert, P.A., and Marcuson, W.F. (1988): Density variation in specimens subjected to cyclic and monotonic loads. Journal of Geotechnical Engineering Division, ASCE, **114**(1): 1-20.

Groot, M.D.B., and Stouthesdijk, T.P. (1997): Undrained stress path of loose sand predicted from dry tests. Canadian Geotechnical Journal, **34**: 131-138.

Hanzawa, H. (1980): Undrained strength and stability analysis for a quick sand. Soils and Foundations, **20**(2): 17-29.

Ichihara, M. (1996): The Osaka group layer and Chinese loess layer (in Japanese). Tokyo: Tsukiji-shokan.

Ishihara, K., Tatsuoka, F., and Yasuda, S. (1975): Undrained deformation and liquefaction of sand under cyclic stresses. Soils and Foundations, **15**(1): 29-44.

Ishihara, K., Okusa, S., Oyagi, N., and Ischuk, A. (1990): Liquefaction-induced flowslide in the collapsible loess deposit in Soviet Tajik. Soils and Foundations, **30**(4): 73-89.

Ishihara, K. (1993): Liquefaction and flow failure during earthquakes. Géotechnique, **43**(3): 39-46.

Kuerbis, R., and Vaid, Y.P. (1988): Sand sample preparation – the slurry deposition method. Soils and Foundations, **28**(4): 107-118.

Martin, G.R., Finn, W.D.L., and Seed, H.B. (1975): Fundamentals of liquefaction under cyclic loading. Journal of Geotechnical Engineering Division, ASCE, **101**(GT5): 423-438.

Matos, M.M. (1988): Mobility of soil and rock avalanches. Ph. D. thesis, Alberta University, Alberta.

Miura, S., and Toki, S. (1982): A sample preparation method and its effect on static and cyclic sand-liquefaction methodologies. Canadian Geotechnical Journal, **29**: 650-665.

Mooney, M.A., Finno, R.J., and Viggiani, M.G. (1998): A unique critical state for sand? Journal of Geotechnical Engineering Division, ASCE, **112**(10): 941-958.

Mulilis, J.P., Seed, H.B., Chan, C.K., and Mitchell, J.K. (1977): Effect of sample preparations on sand liquefaction. Journal of Geotechnical Engineering Division, ASCE, **103**(GT2): 91-108.

Okada, Y., Sassa, K., and Fukuoka, H. (2000): Liquefaction and the steady state of weathered granitic sands obtained by undrained ring shear tests: A fundamental study of the mechanism of liquidized landslides. Journal of Natural Disaster Science, **22**(2): 75-85.

Poulos, S.J. (1981): The steady state deformation. Journal of Geotechnical Engineering Division, ASCE, **107**(GT5): 553-562.

Riemer, M.F., and Seed, R.B. (1997): Factors affecting apparent position of steady-state line. Journal of Geotechnical and Geoenvironmental Engineering Division, ASCE, **123**(3): 281-288.

Sassa, K. (1988): Motion of landslides and debris flows -Prediction of hazard area-. Report of Grant-in-Aid for Scientific Research by Japanese Ministry on Education, Science and Culture (No. 61480062).

Sassa, K. (1995): Keynote Lecture: Access to the dynamics of landslides during earthquakes by a new cyclic loading high-speed ring shear apparatus. In Proceedings of 6th International Symposium on Landslides, "Landslides," Balkema, **1**: 115-132.

Sassa, K. (1996): Prediction of earthquake induced landslides, Special Lecture of 7th International Symposium of Landslides, "Landslides," Balkema, **1**: 115-132.

Sassa, K., Fukuoka, H., Scarascia-Mugnozza, G., and Evans, S. (1996): Earthquake- induced- landslides: Distribution, motion and mechanisms. Special Issue for the great Hanshin Earthquake Disasters, Soils and Foundations, pp. 53-64.

Sassa, K. (2000): Mechanisms of flows in granular soils. Invited paper. Proceedings of GeoEng2000, Melbourne, **1**: 1671-1702.

Sassa, K., Wang, G.H. and Fukuoka, H. (2001): Mechanism of Transition from slide to flow in granular soils. Proceedings of ISSMGE TC-11 (Landslides) Conference on Transition from Slide to Flow – Mechanisms and Remedial Measures -, Trabzon, 1-20.

Seed. H.B., and Lee, K.L. (1966): Liquefaction of saturated sand during cyclic loading. Journal of the Geotechnical Engineering Division, ASCE, **92**(CM6): 105-134.

Seed, H.B. (1979): Soil liquefaction and cyclic mobility evaluation for level ground during earthquakes. Journal of the Geotechnical Engineering Division, ASCE, **105**: 201-255.

Skempton, A.W. (1954): The pore pressure coefficients A and B. Géotechnique, **4**: 143-147.

Sladen, J.A., D'Hollander, R.D., and Krahn, J. (1985): The liquefaction of sands, a collapse surface approach. Canadian Geotechnical Journal, **22**: 564-578.

Sukumaran, B., Leonards, G.A., and Fox, J. (1996): Liquefaction and postliquefaction behaviour of sand. Journal of Geotechnical Engineering Division, ASCE, **121**(2): 502-503.

Vaid, Y.P., Chung, E.K.F., and Kuerbis, R.H. (1990): Stress path and steady state. Canadian Geotechnical Journal, **27**: 1-7.

Yoshimi, Y., Richart, F.E., Prakash, S., Balkan, D.D., and Ilyichev, V.A. (1977): Soil dynamics and its application to foundation engineering. In Proceedings of the 9th International Conference of Soil Mechanics, **2**: pp. 605-650.

Yoshimine, M., and Ishihara, K. (1998): Flow potential of sand during liquefaction. Soils and Foundations, **38**(3): 189-198.

要旨

長距離せん断が可能なリングせん断試験及び三軸圧縮試験において発揮される砂の非排水せん断挙動の解明を目的に，細粒珪砂及び風化花崗岩試料を対象に実験を実施した。また，排水時の摩擦係数と見かけの摩擦係数の比を「高速流動現象ポテンシャル」と定義した。リングせん断試験だけでなく三軸圧縮試験においても，せん断が進み試料中にせん断面が形成されると，粒子の破砕が進行し間隙水圧が上昇するため，高い高速流動現象ポテンシャルを示すことが示された。

キーワード： リングせん断試験，粒子破砕，過剰間隙水圧，せん断抵抗，高速流動ポテンシャル